The Application of Large-Signal Calibration Techniques yields Unprecedented Insight during TLP and ESD Testing

Renaud Gillon (1), Marc Vanden Bossche (2), Frans Verbeyst (2)

(1) ON Semiconductor Belgium BVBA, Westerring 15, 9700 Oudenaarde, Belgium
tel.: +32-55-332702, e-mail: renaud.gillon@onsemi.com, web: www.onsemi.com

(2) NMDG NV, Cesar van Kerckhovenstraat 110, Bldg 5, 2880 Bornem, Belgium
tel.: +32 3 890 46 12, e-mail: info@nmdg.be, web: www.nmdg.be

Abstract – This paper presents the application of a rigorous large-signal calibration technique to TLP waveforms. In contrast to standard practice, which discards information 'hidden' in the transients, the new method allows to visualize currents and voltages occurring at the device-under-test without the distortions which render standard TLP waveforms difficult to interpret.

I. Introduction

The Transmission-Line Pulse technique (TLP) is a well-established characterization method, where the stabilized part of the response to an incoming pulse is exploited to plot one point on a quasi-static I(V) characteristic, [1]. By repeatedly adjusting the amplitude of the pulse, a full characteristic can be plotted, even in regions where the device would fail if tested in DC. The technique owes its success to its simplicity, but recently, several limitations have come under the spotlights.

Trémouilles et al. showed in [2] that damageable dynamic overshoots can be overseen by standard TLP, as only the quasi-static information of the pulse is recorded and the 'noisy' transients are neglected.

This issue even turned into an overwhelming problem when attempting to test large DMOS transistors as described by Coppens et al. in [3]. The TLP pulses were found to trigger damped oscillations which were extending far beyond the usual 10ns rise-time and affecting the values of the quasi-static current and voltage readings of the TLP system. The necessary insight and the resolution of the problem came from the reconstruction of the current and voltage waveforms occurring at the transistor pins, after a lengthy modeling and simulation process [3].

The objective of this paper is to demonstrate how a calibration technique initially developed for the characterization of high-frequency nonlinear devices can be applied to TLP waveforms in order to automatically reconstruct the voltages and currents occurring at the calibration plane. It is believed that the new technique will contribute to speed-up the development of ESD cells.

After a description of basic RF calibration techniques and their limitation, these techniques are extended to large signals and finally their application to TLP and the experimental validation is described.

II. Standard S-parameter calibration techniques

A typical TLP system can be represented from a signal perspective by the schematic shown in Figure 1. This schematic is very similar to the model used for a single-port vector network analyzer (VNA) system, for which various accurate and flexible calibration techniques are available. These calibration techniques use the S-parameter formalism and operate in the frequency domain, relying on the following assumptions :

- Every measurement point is taken with a very narrow bandwidth around a single frequency.
- At every frequency, there exists a linear relationship between the signals of interest and their image acquired by the measuring instrument.

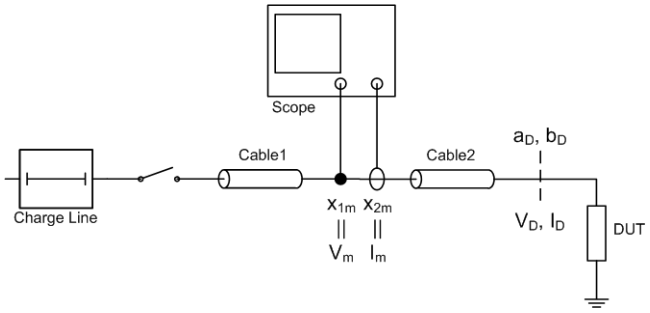

Figure 1: Simplified schematic of the TLP system

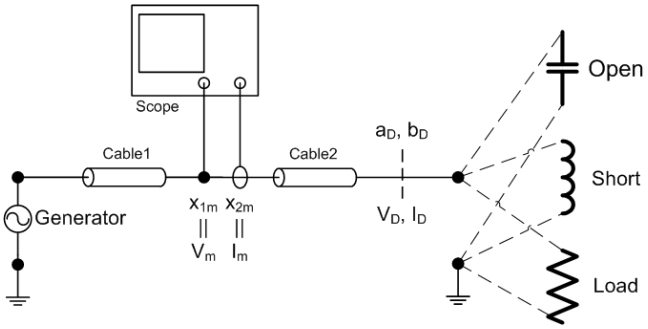

Figure 2: Linear S-parameters calibration using pre-characterized Open, Short and Load standards. The Pulsing Unit is replaced by a RF generator.

- The device-under-test (DUT) operates in the linear regime, and no energy is transferred from the measurement frequency to other frequencies. Typically, this condition is enforced by applying test-signals of sufficiently small amplitude to the DUT. Hence the term 'small-signal operation'.

Figure 2 shows how the TLP system can be adapted for calibration by substituting a RF generator to the pulsing unit. Based on the assumptions listed above, the measurement system can be represented by a set of linear equations which relates the raw readings (x_{1m}, x_{2m}) to the DUT quantities (a_D, b_D) evaluated at the calibration plane :

$$\begin{bmatrix} a_D(\omega) \\ b_D(\omega) \end{bmatrix} = \begin{bmatrix} e_{11} & e_{12} \\ e_{21} & e_{22} \end{bmatrix} . \begin{bmatrix} x_{1m}(\omega) \\ x_{2m}(\omega) \end{bmatrix} \quad (1)$$

where the e_{ij} are the frequency-dependent error-coefficients. In a VNA system, the readings (x_{1m}, x_{2m}) are typically an image of the forward and reflected waves occurring at the measurement port of the VNA and sampled using directional couplers. In the TLP system on the other hand, the readings (x_{1m}, x_{2m}) are an image of the voltage and currents sampled using a pulse transformer and a resistive divider. As long as the pulse transformer does not get saturated, a linear relationship exists at every frequency between the travelling waves and the voltage and current, and the formalism of (1) still applies.

In order to obtain the classical formalism of S-parameter calibration techniques it is necessary to call up on the assumption of 'small-signal' operation, which allows to represent the DUT by a simple frequency-dependent transfer coefficient (the S-parameter) defined as the ratio of the incident and reflected waves a_D and b_D :

$$\Gamma_D = \frac{b_D}{a_D} = \frac{e_{21} \cdot \Gamma_m + e_{22}}{e_{11} \cdot \Gamma_m + e_{12}} \text{ where } \Gamma_m = \frac{x_{2m}}{x_{1m}} \quad (2)$$

As a consequence, only three error coefficients need to be determined in order to be able to make a proper S-parameter calibration, and in most cases e_{11} is eliminated, as shown in equation (3) :

$$\Gamma_D = \frac{b_D}{a_D} = \frac{\beta \cdot \Gamma_m + \gamma}{\Gamma_m + \alpha} \quad \text{with } \alpha = \frac{e_{12}}{e_{11}}, \beta = \frac{e_{21}}{e_{11}}, \gamma = \frac{e_{22}}{e_{11}} \quad (3)$$

This explains that only 3 distinct measurements are required to calibrate a one-port VNA: for example a short, an open and a load. Then defining Γ_{DO}, Γ_{DS}, Γ_{DL} as the a-priori known reflection coefficients of the open, short and load calibration standards repectively, and Γ_{mO}, Γ_{mS}, Γ_{mL} the corresponding readings of the system, the unknown calibration constants α, β, γ can be determined as :

$$\begin{bmatrix} \alpha \\ \beta \\ \gamma \end{bmatrix} = \begin{bmatrix} -\Gamma_{DO} & \Gamma_{mO} & 1 \\ -\Gamma_{DS} & \Gamma_{mS} & 1 \\ -\Gamma_{DL} & \Gamma_{mL} & 1 \end{bmatrix}^{-1} \begin{bmatrix} \Gamma_{DO}\Gamma_{mO} \\ \Gamma_{DS}\Gamma_{mS} \\ \Gamma_{DL}\Gamma_{mL} \end{bmatrix} \quad (4)$$

where the matrix to be inverted is well-conditioned and invertible provided that the calibration standards are appropriately chosen and the corresponding measurements sufficiently distinct. Then using the calibration constants from (4) together with (3), it is possible to correct the measured reflection coefficient of any DUT (Γ_m) for the systematic errors induced by the measurements system and obtain the reflection coefficient of the device (Γ_D) as seen at the calibration plane.

This type of calibration has proven extremely useful for the characterisation of passive components such as resistors, capacitors and inductors showing no significant bias-dependant characteristics. S-parameter techniques are also applied to nonlinear devices such as diodes, field-effect or bipolar transistors, but only operated in small-signal around

some bias-point where they can be characterised by a linear transfer function, and as such the superposition principle holds.

In the case of nonlinear components fed by large-signal waveforms, the amplitude of the current and voltages or the corresponding travelling waves is critical, and the linear S-parameter formalism becomes inappropriate as a description of the device behaviour. The characterisation of nonlinear components requires the ability to reconstruct the exact waveforms occurring at their terminals, [4]. The S-parameters calibration described in this section does not allow to achieve this as it only allows to determine the α, β, γ calibration coefficients, and one complex coefficient is missing at every frequency to be able to reconstruct the $[e_{ij}]$ matrix in equation (1), and hence the waveforms (a_D, b_D) from the measured (x_{1m}, x_{2m}). The following section describes the technique developed at NMDG to extend existing S-parameter calibrations and determine the missing coefficients.

III. Large-signal calibration

In order to be able to reconstruct the exact waveforms occurring at the DUT terminals, it is necessary to determine all elements of the error-coefficients matrix shown in (1). As shown in the previous section, S-parameter calibration techniques allow to determine three calibration coefficients, α, β, γ. The following equation defines the 'missing coefficient' K which must be determined in order to complete the 'large-signal calibration' :

$$\begin{bmatrix} a_D(\omega) \\ b_D(\omega) \end{bmatrix} = K \cdot \begin{bmatrix} 1 & \alpha \\ \beta & \gamma \end{bmatrix} \cdot \begin{bmatrix} x_{1m}(\omega) \\ x_{2m}(\omega) \end{bmatrix} = \begin{bmatrix} e_{11} & e_{12} \\ e_{21} & e_{22} \end{bmatrix} \cdot \begin{bmatrix} x_{1m}(\omega) \\ x_{2m}(\omega) \end{bmatrix} \quad (5)$$

According to [5] and [6], the determination of the coefficient K at all frequencies of interests proceeds in two steps:

- Extraction of its modulus $|K|$ using a power-meter as illustrated in Figure 3.
- Extraction of its phase $\phi = \angle K$ using a special device called 'harmonic phase reference' (HPR), as shown in Figure 4.

For the extraction of the modulus $|K|$, the calibration factor (CF) of the power meter must be taken into account. It is typically specified by the manufacturer, and allows to write the following equations relating the internal reading of the power meter P_S to the incident power at the calibration plane P_D and finaly the module of the travelling wave $|a_D|$:

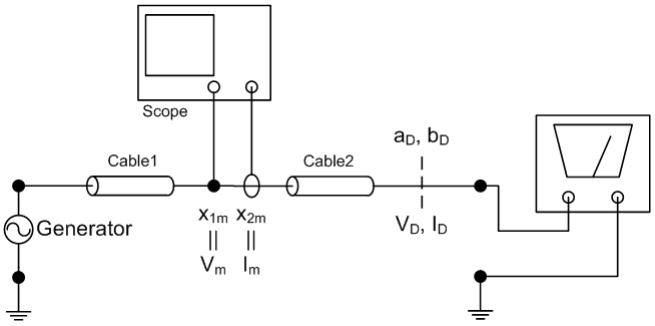

Figure 3: Power-level calibration using a power meter. The Pulsing Unit is replaced by a RF generator.

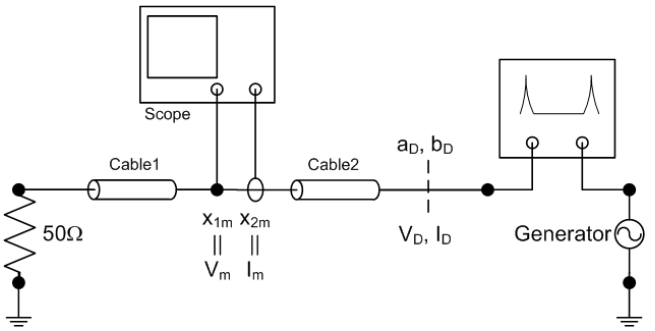

Figure 4: Phase calibration using the Harmonic Phase Reference. The RF Generator generates the input signal for the HPR.

$$P_S(\omega) = CF(\omega) \cdot P_D(\omega) \text{ with } |a_D(\omega)|^2 = P_D \quad (6)$$

Combining equations (5) and (6) , the modulus of K can be easily determined at all frequencies of interest:

$$P_S = CF(\omega) \cdot P_D = CF(\omega) \cdot |K \cdot (x_{1m} + \alpha \cdot x_{2m})|^2$$
$$|K| = \frac{\sqrt{P_S}}{\left|\sqrt{CF(\omega)} \cdot (x_{1m} + \alpha \cdot x_{2m})\right|} \quad (7)$$

In order to extract the ϕ, the phase of K, a reference device is used according to the method described in [6]. The 'Harmonic Phase Reference' (HPR) is connected as shown in Figure 4, and generates a signal appearing as a very short and sharp pulse in the time-domain and corresponding to a comb of harmonics with a known phase in the frequency domain. The pre-characterized phase of the harmonics is used to determine ϕ at the corresponding frequencies. The fundamental of the signal from the HPR is defined by a reference sinusoid obtained from the RF generator which can be swept to extract ϕ on different frequency grids. Additionally, ϕ can be interpolated to limit the number of required HPR measurements.

Taking into account the reflection coefficient of the HPR and the different harmonic components of its

signal, the signals at the calibration plane can be expressed as follows :

$$b_D(\omega) = \Gamma_H(\omega) \cdot a_D(\omega) + a_H(\omega) \quad (8)$$

Then using equation (5), the ϕ can be extracted :

$$K(\omega) = a_H \cdot (x_{1m} \cdot (\beta - \Gamma_H) + x_{2m} \cdot (\gamma - \alpha \cdot \Gamma_H))^{-1} \quad (9)$$

$$\angle K(\omega) = \angle a_H - \angle[x_{1m} \cdot (\beta - \Gamma_H) + x_{2m} \cdot (\gamma - \alpha \cdot \Gamma_H)] \quad (10)$$

Once that both the phase and the modulus of K are extracted at all frequencies of interest, equation (5) can be used to convert the spectra of the raw measured quantities (x_{1m}, x_{2m}) into the spectra of the waves (a_D, b_D) at the terminal of the DUT or equivalently, the spectra of the current and voltages at that point using the usual conversion formula :

$$\begin{aligned} \begin{bmatrix} v_D(\omega) \\ i_D(\omega) \end{bmatrix} &= \begin{bmatrix} 1 & 1 \\ \frac{1}{Z_0} & \frac{-1}{Z_0} \end{bmatrix} \cdot \begin{bmatrix} a_D(\omega) \\ b_D(\omega) \end{bmatrix} \\ &= \begin{bmatrix} 1 & 1 \\ \frac{1}{Z_0} & \frac{-1}{Z_0} \end{bmatrix} \cdot K \cdot \begin{bmatrix} 1 & \alpha \\ \beta & \gamma \end{bmatrix} \cdot \begin{bmatrix} x_{1m}(\omega) \\ x_{2m}(\omega) \end{bmatrix} \end{aligned} \quad (11)$$

The above procedure will be called 'four-term error correction', owed to the four frequency-dependent coefficients K, α, β, γ. The complete procedure used to correct the TLP waveforms, including the Fourrier Transforms required to map the scope waveforms to frequency domain data is illustrated in Figure 5, and is discussed in the next section.

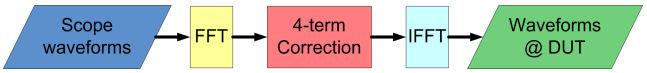

Figure 5: Main steps for the proposed correction technique

IV. Application to TLP

To apply the calibration procedures described in the previous sections to the TLP system, the hardware described in Table 1 was used. Before starting any practical measurement, the system must be configured by selecting the time-window, the frequencies at which to calibrate and the range of the oscilloscope to use during the calibration.

- In order to capture sufficient information about multiple reflections of the TLP pulse, a time-window of 400ns was selected. This yields a fundamental frequency of 2.5MHz, the multiples of which define the frequency grid that will be used for the S-parameter calibration.
- The Celestron-I system uses a resistive divider to sample the voltage of the TLP pulse, which requires a 1MΩ input impedance for the scope channel. This is realized using a TCA-1MEG adapter, which however limits the bandwidth of the system to ~ 500MHz. As a result, a total of 200 equally spaced frequency points were selected for the S-parameter calibration running from 2.5MHz till 500MHz.
- Next, connecting the HPR according to Figure 4 and powering it at its optimal operating point according to the manufacturer's guideline, the appropriate scope ranges on the channels for (x_{1m}, x_{2m}) were selected. Finally, the RF generator is connected as in Figure 3, and its output power-level is adjusted to the largest value ensuring that none of the scope channels go out of range at any of the calibration frequencies – corresponding to a level 6dBm.

Then once the system is configured, the S-parameter calibration is executed at all frequency points according to the procedure described in Section II and Figure 2. Then the modulus of K is extracted at all frequency points executing the power calibration described in Section III with the connection shown in Figure 3.

Finally, using the setup from Figure 4, the phase-calibration is performed and the phase of K at all frequencies corresponding to the harmonics generated by the HPR using an excitation signal (and fundamental frequency) of 15MHz. This frequency is selected according to internal constraints of the HPR, and generates a frequency grid which is a subset the one used for the S-parameter calibration.

Table 1: Equipment used for the TLP calibration at ONSEMI

Equipment	*Manufacturer*	*Model*
Base TLP	Oryx	Celestron-I 100ns pulse
Sampling scope	Tektronix	DPO70404 4GHz – 20Gs + TCA-1MEG
RF Generator	Rhode & Schwarz	SMA100A 9kHz – 6GHz
HPR	NMDG	NM300
SMA Calkit	Agilent	85052D 3.5 mm
Cal. substrate	GGB Industries	CS5
RF Probes	GGB Industries	Picoprobes Model 40 GSG

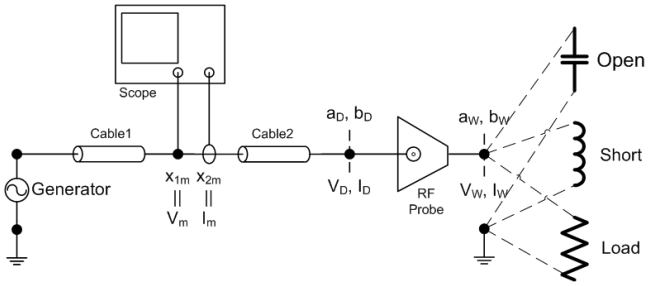

Figure 6: Transfer of the calibration plane towards the probe-tips.

As a result, the phase of K must be interpolated towards the missing frequency points in order to cover all frequencies required for the correction of the TLP waveforms. A study conducted in the frame of the present work, showed that the interpolation of $\phi(\omega)$ worked best when formulating the calibration equations using travelling waves as in Section II, instead of the corresponding voltages and currents. İt was found that in a formulation of equation (5) using $(v_D,\ i_D)$ instead of $(a_D,\ b_D)$, the equivalent $\phi(\omega)$ showed much stronger frequency variations with many zeros and poles, such that applying interpolation was not possible.

After completion of all preceding steps, the system is calibrated with a DUT plane corresponding to the mating plane of the SMA connectors used to connect the cables to the calibration elements and the various pieces of equipment. However, the TLP system is mostly used to characterize on-wafer components, and the calibration plane must be moved to the probe tips. Therefore, a second S-parameter calibration is realized using on-wafer probes and an alumina calibration substrate, allowing to extend the large-signal calibration towards the probe tips. The extension of the large-signal calibration to the probe-tips requires to determine the four elements of the transfer matrix linking the waves $(a_D,\ b_D)$ to those at the tips, $(a_W,\ b_W)$. As it is not possible to execute the power and phase calibrations on-wafer, one must revert to the assumption that the probes are passive and reciprocal, which yields an additional constraint allowing to determine the K coefficient, [6].

All the operations described in this section were programmed using the ICE framework developed by NMDG, [7], and the user is guided through the different calibration steps by the calibration 'wizard' integrated in the graphical user interface.

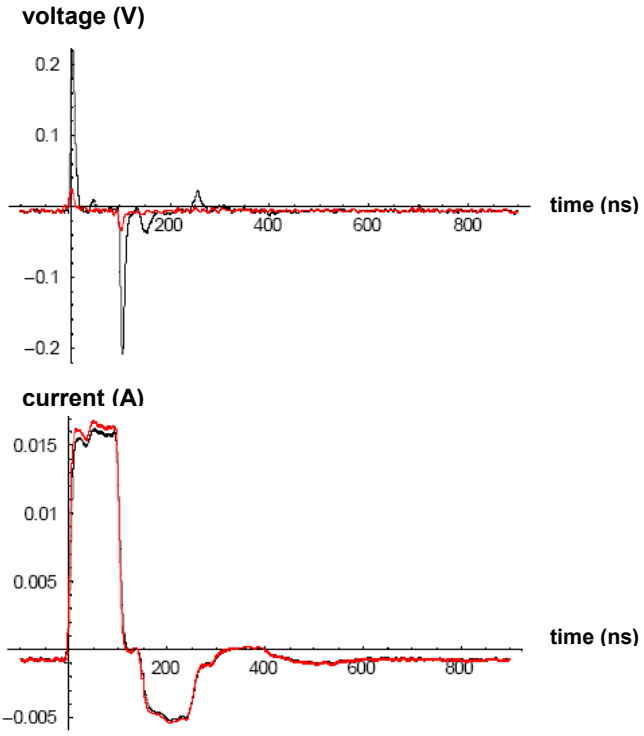

Figure 7: Validation of the large-signal calibration on a connectorized short standard (Black : w/o calibration; Red : with).

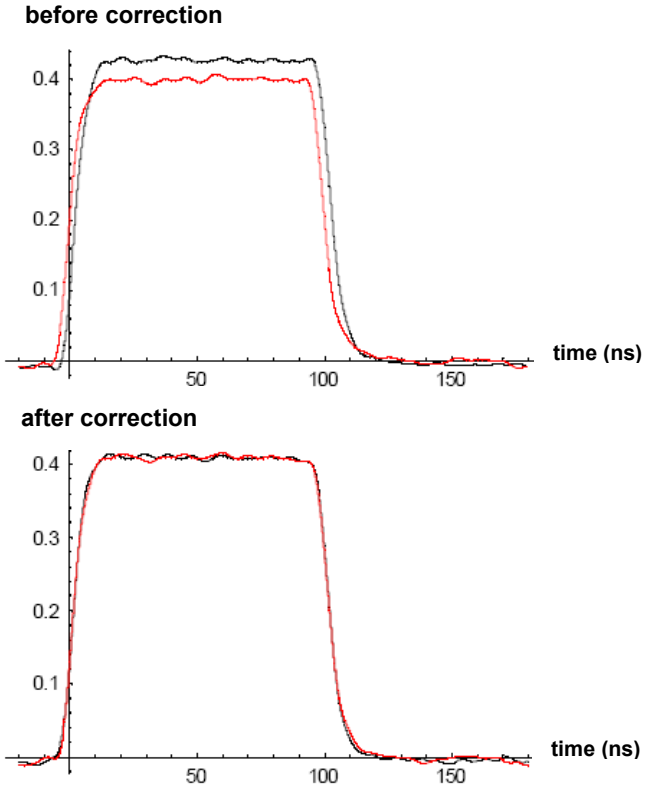

Figure 8: Validation of the large-signal calibration on a connectorized 50Ohm standard (Black : voltage waveform; Red : current x50 waveform).

V. Results

In order to assess the feasibility of applying the large-signal calibration to our TLP system, some tests were performed in a connectorized environment. Figure 7 shows how the calibration 'improves' the response of a short circuit, minimizing the spurious voltage peaks. The residual inductance after calibration evaluates to ~1nH, which is very reasonable for a coaxial offset-short standard (K-type connectors). Figure 8 shows the response of a 50Ω resistor. After calibration the voltage and the current waveform multiplied by 50 overlap quasi-perfectly, demonstrating the validity of the calibration approach.

On-wafer experiments were realized subjecting the drain of a grounded-gate low-voltage NMOS to 15V TLP pulses. Figure 9 shows the time-domain waveforms before and after calibration. One can clearly see that, on the calibrated waveforms, the current rises quickly as soon as the voltage exceeds 9V in good agreement with the expected physical behaviour of the device.

Figure 10 shows the same data in the state-space plane where one can also recognize the distinctive features of snap-back. The calibration method currently does not include DC. For the time being, DC information is added assuming zero voltage and current at time 0. Work is ongoing to add calibrated DC information.

VI. Conclusion

This paper reported on the application of a large-signal calibration technique to TLP waveforms for the first time, allowing to visualize the dynamic currents and voltages occurring at the device under test. This technique will reveal previously hidden details of the behaviour of the DUT, enabling ESD engineers to make more precise diagnostics of the situation and to speed up the development of ESD protections. It is expected that this technique will also be very useful for the large-signal characterization of high-speed devices, in both single-port and multi-port configurations.

Future work will involve evaluating various hardware simplifications as replacing RF probes by more popular needle probes, making use of the pulses generated by the charge-line for the phase calibration, and testing the method on other kind of testers (HBM or systemESD for example).

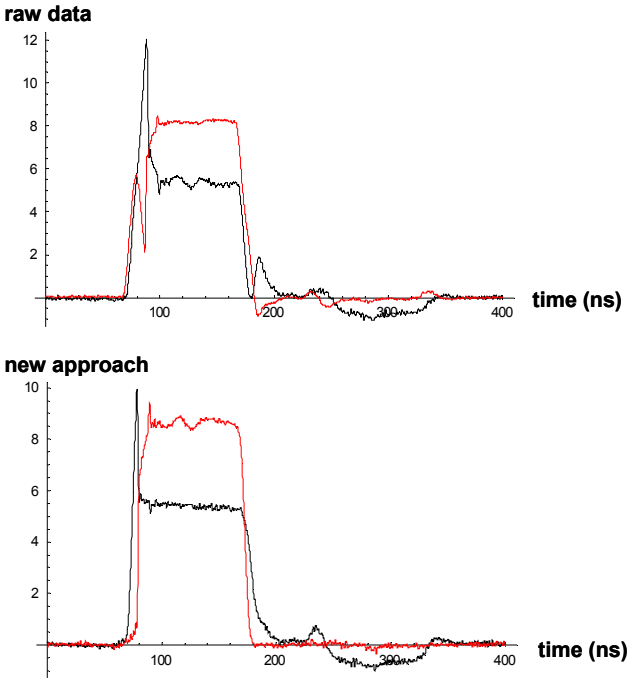

Figure 9: Dynamic TLP voltage (black) and Current x 50 (red) waveforms recorded on a Grounded-Gate NMOS transistor, before (Top) and after correction (bottom).

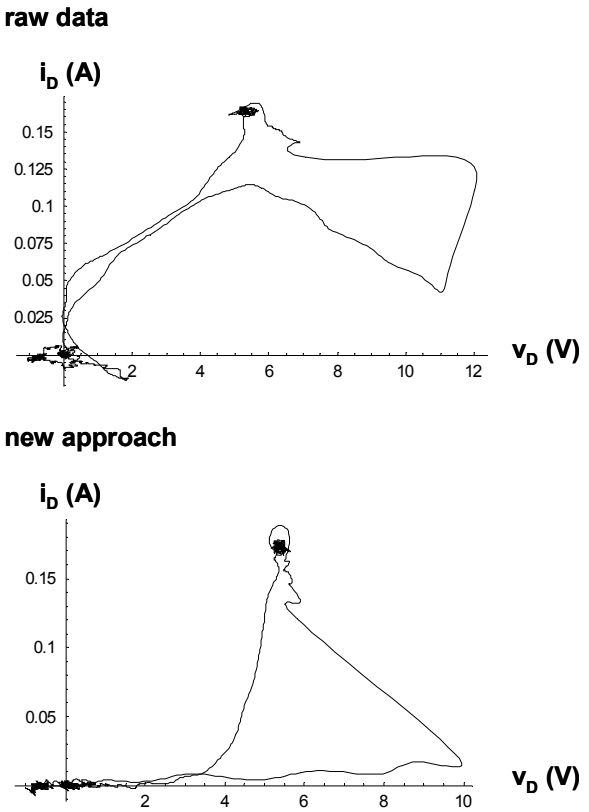

Figure 10: Dynamic TLP waveforms plotted in I(V) state space, before (top) and after (bottom) calibration. Snapback to ~5.0V occurs just above 9V.

Acknowledgements

This work was partly funded by the Flemish Region (IWT) in the frame of project FIETS.

References

[1] J. E.Barth, K. Verhaege, L. Henry, J. Richner, "TLP Calibration, Correlation, Standards, and New Techniques", Tran. on Electronics Packaging Manufacturing, Vol. 24, no. 2, April 2001, pp. 99-107.

[2] D. Trémouilles, S. Thijs, Ph. Roussel, M.I. Natarajan, V. Vassilev and G. Groeseneken, "Transient Voltage Overshoot in TLP testing – Real or Artifact?", Microelectronics Reliability, Volume 47, Issue 7, July 2007, pp 1016-1024

[3] P. Coppens, , G. Jenicot, H. Casier, F. De Pestel, F. Depuydt, N. Martens and P. Moens, "TLP Characterization of large gate width devices", Microelectronics Reliability, Volume 47, Issues 9-11, Sep.-Nov. 2007, pp. 1462-1467

[4] U. Lott, "Measurement of Magnitude and Phase of Harmonics Generated in Nonlinear Microwave Two-Porst", IEEE Trans. Microw. Theory Tech., vol. 37, no. 10, pp. 1506–1511, Oct. 1989.

[5] M. Vanden Bossche, A. Barel, "Theoretical Aspects of Calibration Procedures in Network Analyzers for Nonlinear One-port Devices" Instrumentation and Measurement Technology Conference, 1990, IMTC-90 Conference Record, 7th IEEE, 13-15 Feb. 1990, pp. 367-372.

[6] J. Verspecht, "Calibration of a measurement system for high frequency nonlinear devices," Ph.D. dissertation, Dept. ELEC., Vrije Univ. Brussel, Brussels, Belgium, 1995.

[7] "Integrated Component Characterization Environment (ICE)", NMDG application note, available at : http://www.nmdg.be/ICE.html